Endometrial stromal cell signaling and microRNA exosome content in women with adenomyosis

Running title: Stroma-derived miRNA exosomes in adenomyosis

Margherita Zipponi[1], Luciana Cacciottola[1], Alessandra Camboni[1,2], Christina Anna Stratopoulou[1], Hugh S. Taylor[3] and Marie-Madeleine Dolmans[1,4,*]

[1]Pôle de Gynécologie, Institut de Recherche Expérimentale et Clinique, Université Catholique de Louvain, Brussels, Belgium
[2]Department of Pathology, Cliniques Universitaires Saint-Luc, Brussels, Belgium
[3]Department of Obstetrics, Gynecology and Reproductive Sciences, Yale School of Medicine, New Haven, CT, USA
[4]Gynecology Department, Cliniques Universitaires Saint-Luc, Brussels, Belgium

*Correspondence: Pôle de Gynécologie, Institut de Recherche Expérimentale et Clinique, Université Catholique de Louvain, Avenue Mounier 52, 1200 Brussels, Belgium. https://orcid.org/0000-0002-6331-3026 marie-madeleine.dolmans@uclouvain.be

Abstract

Adenomyosis is a chronic, estrogen-driven disorder characterized by the presence of endometrial glands and stroma within the myometrium. Despite its significant impact on reproductive health and quality of life, the pathogenesis of the disease remains unclear. Both the glandular and stromal compartments of eutopic endometrium from women with adenomyosis show alterations compared to healthy subjects. However, the molecular mechanisms driving crosstalk between stromal cells and epithelial glands, along with paracrine signaling underlying lesion development and progression, are still poorly understood. Exosomes, small cell-derived carriers and microRNAs, namely non-coding RNA molecules, are crucial to intercellular communication within the endometrium and may elucidate interactions between the two compartments that contribute to adenomyotic lesion formation. To our knowledge, this is the first foundational study to comprehensively isolate and characterize stroma-derived exosomes from women with adenomyosis. Exosome isolation by means of differential ultracentrifugation was validated in 22 samples, including 11 healthy subjects and 11 women with adenomyosis, using nanoparticle tracking analysis, transmission electron microscopy and flow cytometry. Profiling of microRNA in secreted exosomes revealed 10 microRNAs with significantly altered expression in adenomyosis subjects during the menstrual phase compared to controls. Thorough investigations into menstruation-specific molecular mechanisms, as well as predicted target genes and enriched pathways of exosomal microRNAs, offer promising insights into the pathogenesis of adenomyosis, shedding light on the potential mechanisms underlying stromal cell signaling and adenomyotic lesion establishment.

This work does, however, have certain drawbacks, including modest sample size and limited representation due to a lack of readily available endometrial biopsies in the

menstrual phase. Having done the groundwork in this study, future research should seek to validate these findings in larger cohorts and apply functional assays. Indeed, our findings can serve as a resource to elucidate the role of menstruation-specific stroma-derived microRNA-mediated signaling and its potential impact on adenomyosis development.

Keywords: adenomyosis / endometrium / endometrial stromal cells / endometrial cell crosstalk / paracrine signaling / exosomes / microRNA / small RNA sequencing.

Introduction

Adenomyosis is a common and chronic estrogen-driven disorder (Chapron et al., 2020; Vannuccini and Petraglia, 2019). Its prevalence in women of reproductive age ranges from 20% to 35% (Naftalin et al., 2012; Pinzauti et al., 2015), but higher rates have been observed in patients with endometriosis-associated pain and concurrent infertility (Upson and Missmer, 2020). Adenomyosis is histologically characterized by irregularly shaped islands of endometrial glands surrounded by stroma accompanied by smooth muscle hyperplasia and hypertrophy within the myometrium (Chapron et al., 2017; Antero et al., 2020). Despite having a major impact on women's reproductive health and quality of life, the aetiology and pathogenesis of adenomyosis have not yet been elucidated (García-Solares et al., 2018; Zhai et al., 2020; Cheng et al., 2023). Growing evidence indicates that some eutopic endometrial cells develop distinct cellular and/or molecular changes driving the development of adenomyosis. This favours: (i) a pro-survival phenotype involving increased endometrial cell proliferation and reduced apoptosis (Yang et al., 2007; d'Argent et al., 2023); (ii) a transition to core features such as altered hormone

levels, specifically a disruption of steroidogenesis, with greater estrogen production and progesterone resistance (Chen et al., 2010), and epithelial-to-mesenchymal transition of epithelial glands and endometrial stromal cells (ESCs) (Khan et al., 2015); and (iii) an invasive phenotype due to collective cell migration (Zhai et al., 2022; Stratopoulou et al. 2023), dysregulated extracellular matrix function, enhanced angiogenesis and impaired immune function (Bourdon et al., 2021). Indeed, endometrial stroma may play a crucial role in adenomyotic lesion establishment, supporting epithelial gland migration into the myometrium, as well as growth and survival via paracrine signaling (Zipponi et al., 2024a). Extracellular vesicles are key mediators of intercellular communication between neighbouring cells and even distant tissues and have been detected in almost all human cells and biofluids, including the endometrium. According to the latest guidelines from MISEV2024, exosomes are extracellular vesicles from internal compartments of the cell that are released by multivesicular bodies (Welsh et al., 2024). These bioactive bilayer membrane nanoparticles constitute a more refined system of cell-cell communication via transfer of proteins, nucleic acids and metabolites to recipient cells in the endometrial microenvironment. As such, they are able to influence cell fate, function and plasticity (Zhang et al., 2019). They contain microRNAs (miRNAs), a type of endogenous non-coding RNA that modulates both physiology and pathology by suppressing target gene expression post-transcriptionally. miRNAs are promising biomarkers thanks to their simple structure and stability at the post-translational level and in extracellular biofluids (Nguyen et al., 2016; Chen et al., 2020). Ongoing research into exosomes and their miRNA content highlights their potential for revolutionizing diagnostics and investigations into cell damage mechanisms across various disorders, including adenomyosis (Zhou et al., 2015; Esfandyari et al., 2021; Cheng et al., 2023). Understanding the exact role of stroma-

derived exosomes and miRNA exosome cargo may shed light on the crosstalk that occurs between stromal cells and glands in the endometrium, ultimately helping to explain adenomyotic lesion development.

We hypothesize that exosomes released from ESCs contribute to the pathogenesis of adenomyosis by carrying and delivering specific miRNAs in an autocrine and paracrine manner. This could further boost the crosstalk between stromal and epithelial compartments and promote lesion establishment and progression.

Materials and methods

Study participants and tissue collection

Human tissue for this study was collected, with informed consent, in accordance with the Declaration of Helsinki guidelines and approved by the ethics committee of Cliniques Universitaires Saint-Luc (CUSL) and the Université Catholique de Louvain on August 31, 2020, and amended on July 23, 2023 (ref: 2020/14AOU/410). A total of 22 fresh endometrial biopsies were retrieved from CUSL patients by means of a Novak curette. The control group included 11 patients with no sign of adenomyosis, endometriosis or any other endometrial pathology. The adenomyosis group was made up of 11 patients diagnosed by magnetic resonance imaging (MRI) or transvaginal sonography (TVS). Seven of these women underwent hysterectomy for symptomatic adenomyosis and four patients underwent conservative surgery for other gynecological indications. All patients were premenopausal with regular menstrual cycles and had not been given any hormonal therapy (contraceptive pill, progestin, gonadotropin-releasing hormone (GnRH) agonist/antagonist implant or hormonal intrauterine device) for at least two months prior

to surgery. One small tissue fragment was fixed in paraformaldehyde for histological evaluation of the menstrual phase, while the rest were used for endometrial cell isolation.

Endometrial cell isolation and culture

Biopsies retrieved from the operating room were immediately placed in cold sterile phosphate-buffered saline (PBS) pH 7.4 (Thermo Fisher Scientific, Waltham, MA, USA) until use. They were processed according to an established protocol (Defrère et al., 2005). Briefly, the tissue was mechanically minced with surgical scissors and enzymatically digested in 1 mg/ml collagenase (Sigma, St. Louis, MO, USA) for one hour. The suspension was strained through a 300-µm sieve to exclude undigested fragments, followed by a 100-µm filter to separate epithelial glands and ESCs. ESCs passing through the sieve were centrifuged for 5 minutes at 82 g and resuspended in Dulbecco's modified Eagle medium F-12 nutrient mixture (DMEM/F-12) (Thermo Fisher Scientific) enriched with 10% heat-inactivated fetal bovine serum (FBS) (Thermo Fisher Scientific) and 1% antibiotic-antimycotic (Thermo Fisher Scientific). After 20 minutes, the medium was replaced with a fresh mixture to exclude blood cells and any residual epithelial cells. The ESCs were cultured at 37°C with 5% CO_2 for expansion, with medium replacement every 2 days.

The ESC phenotype was tested before adding exosome-depleted FBS to the culture medium (10%) by immunocytochemistry on five representative samples. After fixation in 4% paraformaldehyde, 300 µL resuspended cells ($5x10^4$ – $5x10^5$ cells/ml) were aggregated on slides using the Shandon Cytospin 2 (Thermo Fisher Scientific) for 10 minutes at 40 g, then stained with mouse anti-human CD10 antibody (ready to use, Sanbio, Uden, the Netherlands). The universal negative mouse cocktail (ready to use, Dako, Carpinteria, CA, USA) was utilized instead of the primary antibody for negative

controls. Ishikawa cells (epithelial-like cell line, Merck, Rahway, NJ, USA) were also used for the same purpose. Human endometrium served as positive controls. Culture purity was 92% (91.8 ± 1.79) (Supplementary Figure S1).

Exosome isolation from ESCs by ultracentrifugation

ESCs were cultured in exosome-depleted FBS for 48 hours based on three considerations: i) ESC medium is routinely changed every 2 days; ii) after culturing ESCs in EV-depleted FBS for both 48 and 72 hours higher exosome concentrations were observed at 48 hours; and iii) exosome secretion tends to decrease as cells approach confluency, so the 48-hour culture period was chosen for optimal exosome collection. FBS used for culture was subjected to ultracentrifugation at 11981 g for 16 hours at 4°C (Ti70 21U8118 rotor, Optima XPN-80, Beckman Coulter, Brea, CA, USA) to eliminate exosomes. To confirm particle depletion, flow cytometry analysis was conducted. PE anti-human CD9 antibody and APC anti-human CD81 TAPA-1 (BioLegend, San Diego, CA, USA), two widely known exosome biomarkers, were used. The supernatant was then filtered (0.22 μm) and stored at -20°C prior to use (Supplementary Figure S2). ESC supernatant was collected from each sample at the end of culture. Differential ultracentrifugation was performed to purify and isolate exosomes according to an established protocol (Zipponi et al., 2024b). Briefly, culture medium was centrifuged twice (Sigma 2-16PK, Merck) at 760 g for 10 minutes at room temperature to remove the bulk of the cell debris. The supernatant was then ultracentrifuged (Optima XPN-80, Beckman Coulter) at 2710 g for 20 minutes at 4°C (Ti50 E4280 rotor, Beckman Coulter) and 11985 g for 120 minutes at 4°C (Ti80 1377 rotor, Beckman Coulter). After discarding the supernatant, the pellets were resuspended in 1 ml 0.22-μm-filtered PBS. Finally, the samples were subjected to ultracentrifugation at 11985 g for 120 minutes at 4°C (Ti80

177 1377 rotor, Beckman Coulter) to obtain pellet particles. Half of the particles were
178 resuspended in 200 µL PBS for exosome characterization by nanoparticle tracking
179 analysis (NTA), transmission electron microscopy (TEM*)* and flow cytometry. The rest
180 were resuspended in 800 µL QIAzol lysis reagent (Qiagen, Hilden, Germany) for RNA
181 extraction. Total RNA was extracted using the miRNeasy mini kit (Qiagen) according to
182 the manufacturer's instructions. Of the remaining RNAse-free water, 2µL were kept for
183 quantification by Quant-IT RiboGreen RNA assays kit (Thermo Fisher Scientific). The
184 RNA was stored at −80°C prior to sequencing. Maximum storage time of RNA samples
185 was 3 months.

186 Particle characterization

187 NTA (ZetaView Particle-Metrix, Dusseldorf, Germany) was used to evaluate extracellular
188 vesicle concentrations and size distribution by visualizing exosomes based on light
189 scattering and Brownian motion. Particle pellets of 5µL were diluted in 0.22-µm-filtrated
190 PBS (1:100 to 1:600), which was used as the blank.

191 To determine exosome morphology, a drop of particle pellets (around 10 µL) was placed
192 on top of 200-mesh Formvar/carbon copper grids. After three washes in deionized water
193 (10 µL/time), the exosomes were steeped in a drop of R1000 UA-Zero (Agar Scientific,
194 Rotherham, UK) for 7 minutes. Once the grid was completely dry (around 15 minutes),
195 the particles were further scrutinized and photographed by TEM using a Zeiss EM10
196 electron microscope operating at 80 kV (Zeiss, Oberkochen, Germany).

197 To investigate exosome biomarkers, particles were stained with CD9 and CD81
198 antibodies. Extracellular vesicle pellets resuspended in carboxyfluoroscein succinimidyl
199 ester (CFSE) (BioLegend, San Diego, CA, USA) and PBS were incubated in 1.5 µL CD9
200 and 1 µL CD81 overnight prior to detection. CFSE-only incubated exosomes were used

as negative controls. Samples were acquired with the NovoCyte Quanteon flow cytometer (Agilent, Santa Clara, CA, USA).

miRNA library preparation and sequencing

Library preparation was done using the QIAseq miRNA Library Kit (Qiagen). Samples of 10 ng of total RNA were converted into miRNA NGS libraries. After adapter ligation, unique molecular identifiers (UMIs) were introduced during the reverse transcription step, before cDNA amplification using PCR (19 cycles), with indices added to this step. Samples were subsequently purified. Library preparation quality was assessed by capillary electrophoresis (Tape D1000). Based on insert quality and concentration measurements, the libraries were pooled at equimolar ratios. Library pools were quantified using qPCR and sequenced on a NextSeq (Illumina Inc., San Diego, CA, USA) sequencing instrument according to the manufacturer's instructions (1x75, 2x10).

miRNA-seq data processing and analysis

Raw data were de-multiplexed, and FASTQ files were generated for each sample using bcl2fastq2 software (Illumina Inc.). All primary analysis was conducted with CLC Genomics Server 23.0.5. using the 'QIAseq miRNA quantification' workflow with standard parameters to map sequencing reads to miRBase version 22 (prioritizing the *Homo sapiens* species).

In brief, the reads were processed by: (i) trimming the common sequence (AACTGTAGGCACCATCAAT, 19 nucleotides), UMI and adapters, and (ii) filtering with length <15 or >55 nucleotides. They were then deduplicated using their UMI. Reads were organized into UMI groups when they: (1) started in the same position based on the end of the read to which the UMI was ligated, (2) came from the same strand, and (3) had identical UMIs. Groups that contained only one read (singletons) were merged into non-

singleton groups if the singleton's UMI could be converted to a UMI of a non-singleton group by introducing an SNP (the largest group was chosen). Distribution of lengths of trimmed reads showed a peak at 22 nucleotides, suggesting that the captured RNA population was potentially enriched in miRNAs.

The total number of libraries prepared, processed and analyzed as reported in this study corresponds to women with adenomyosis in the menstrual phase (age range 41-47) and healthy individuals also in this phase (age range 36-40). Mapping the reference allowed us to identify 2632 miRNAs used for further exploration. Read counts were transformed into counts per million (cpm) to account for overall sequencing depth and serve as an indicator of expression levels. Fold changes were calculated as expression in adenomyosis over healthy samples. miRNAs of interest between healthy and adenomyosis samples were identified by investigating fold changes in expression: $\log_2$ fold change >2 and <-2.

Validation of miRNA expression and enrichment analyses

In order to validate expression of these selected miRNAs, 8 endometrial biopsies from women in the menstrual phase with (n=4) and without (n=4) adenomyosis were used. Exosomes were isolated from ESCs and RNA was extracted and quantified following the protocol described above. First-strand cDNA synthesis was performed using the miRCURY LNA RT kit and GeneAmp 9700PCR system (Applied Biosystems, Foster City, CA, USA). In line with the manufacturer's protocol, the following cycling program was developed: 60 minutes at 42°C (reverse transcription step) and 5 minutes at 95°C (reaction inactivation). Synthesized cDNAs were stored at -20°C for further detection of miRNA targets. MiRCURY LNA miRNA custom PCR panels (SYBR green-based detection, Qiagen) were utilized to ensure high specificity for miRNA expression level

quantification. CDNA templates were diluted (1:80) prior to use according to the manufacturer's protocol. The StepOnePlus real-time PCR system (Applied Biosystems) was set up with the following thermocycling conditions: 2 minutes at 95°C (initial heat activation), 10 seconds at 95°C (denaturation), and 60 seconds at 56°C (combined annealing/extension) for 40 cycles. Experiments were performed in duplicate. ROX reference dye was used at a ratio of 20x concentration for each fluorescence normalization reaction. SNORD38B, UniSP3 and 7 endogenous miRNAs were utilized as references (miR-28-3p, miR-151a-3p, miR-421, miR-574-5p, miR-93-5p, miR-15b-5p and miR-99b-3p) and uniSp6 was used as an internal amplification control (Supplementary Table S1).

miRNA target retrieval

The miRNet platform (miRBase and miRTarBase v8.0) (https://www.mirnet.ca/miRNet/home.xhtml, University of Alberta, Edmonton, AB, Canada) allowed us to retrieve information about predicted target genes of dysregulated miRNAs. Gene ontology (GO) enrichment analysis was carried out via ShinyGO v0.80 (http://bioinformatics.sdstate.edu/go/, South Dakota State University, Brookings, SD, USA), yielding insights into high-level classification of the functional role of predicted target genes. The GO biological process was used as a pathway database, with 0.01 as the false discovery rate (FDR) cut-off. The g:Profiler web server (University of Tartu, Tartu, Estonia) provided comprehensive functional enrichment analysis and detailed information about specific molecular interactions and processes that are overrepresented in a given set of genes, namely predicted target genes for the first ten GO terms. KEGG, Reactome and WikiPathways were applied as data sources for g:Profiler and the Benjamini-Hochberg FDR, and 0.01 as the threshold.

Statistical analyses

Statistical analyses were performed using GraphPad Prism 8.0.1 (GraphPad Software, San Diego, CA, USA). Data are presented as means ± SD. The unpaired t-test was conducted for flow cytometry results and GeneGlobe for PCR data analysis (Qiagen, Hilden, Germany). The paired t-test and 2-tail p-value were calculated between the two groups, and the global threshold cycle (Ct) mean of expressed miRNAs was used as a normalization method. As the lower limit of detection, a Ct cut-off value of 36 was adopted. P-values were determined based on Student's t-test for each miRNA in the control group and adenomyosis group, with p-values of <0.05 and <0.01 respectively considered statistically significant.

Results

Characterization of stroma-derived exosomes

NTA was conducted to assess particle diameter and concentration. Purified exosomes from ESC supernatant from both adenomyosis and healthy subjects showed a 50-200 nm size range (179.5 ± 72) and a 4.5-19E+10 particles/ml concentration range (9.6E+10 ± 4.9E+10 and 10.6E+10 ± 4.4E+10 respectively) (Figure 1A). No measurable differences were observed in exosome size or yield (Supplementary Figure S3A). They appeared as cup-shaped bimembrane structures, often with a thin and highly electron-dense membrane upon TEM (Figure 1B). Exosome biomarkers (CD9, CD81) were detected in purified stroma-derived particles by flow cytometry (Figure 1C). Statistical analyses found no difference in numbers of CD9-positive and CD81-positive particles between healthy and adenomyosis subjects, indicating that ESCs from women with and without

adenomyosis release the same numbers of exosomes (Supplementary Figure S3B-S3C). These findings confirm that stroma-derived particles are indeed exosomes.

miRNA sequencing and data validation by qPCR

Regarding small RNA (miRNAs, long non-coding RNAs, mitochondrial RNA, ribosomal RNA, other), the distribution percentages in control and adenomyosis samples were 42% and 37% respectively, representing the largest proportion of total small RNA, with no significant difference between groups (Supplementary Figure S4). To establish qualitative changes in miRNA expression profiles, fold changes were explored. No differential changes in miRNA expression were observed between the three different phases of the cycle in the pooled cohort of samples (n=8 proliferative, n=7 secretory, n=2 menstrual). There were also no differences in miRNA expression between controls and adenomyosis patients during the proliferative or secretory phases (4 adenomyosis and 4 healthy in the proliferative phase and 3 adenomyosis and 3 healthy in the secretory phase). However, changes in miRNA expression were noted between healthy and adenomyosis subjects during the menstrual phase, yielding a functional sample.

Of 2632 miRNAs detected, 38 were considered candidates of interest according to the following parameters: $\log_2$ fold change >2 and <-2 and count per million (Supplementary Table S1). Among these 38 miRNAs, 14 were increased and 22 decreased in stroma-derived exosomes isolated from adenomyosis patients compared to healthy subjects during the menstrual phase (Figure 2).

Changes miRNA expression was then validated by qPCR on 8 more samples of endometrial biopsies retrieved from the menstrual phase (Supplementary Table S1). Of the 38 miRNAs investigated, 12 exhibited a relatively high (>30) average Ct (more than five cycles below the cut-off), meaning that their relative expression level was low in both

groups and the fold change p-value was either unavailable or relatively high. Finally, 10 miRNAs showed significantly different expression levels between affected and healthy subjects in the menstrual phase. Specifically, miR-132-5p, miR-451a and miR-99a-5p were upregulated, while miR-431-3p, miR-29c-39, miR-337-5p, miR-144-3p, miR-590-3p, miR-1275 and miR-7-5p were downregulated (Table 1).

Gene set enrichment and functional analyses

Systematic analysis was conducted to comprehensively scrutinize potential regulatory mechanisms and uncover pathways underlying biological processes associated with the 10 miRNAs showing statistically different expression, validated by qPCR on biopsies of menstrual endometrium. The most common target genes shared by three miRNAs of interest were BCL2, BTG anti-proliferation factor 2 (BTG2), ataxin-1 (Akt signaling), aminoethanethiol dioxygenase (ADO), insulin-like growth factor 1 receptor (IGF1R), nucleus accumbens-associated 1 (NACC1), pleckstrin homology domain-containing A3 (PLEKHA3), SUZ RNA binding domain containing 1 (SZRD1) and Tet methylcytosine dioxygenase (TET). The top GO terms for the biological process category were intrinsic apoptotic signaling pathways in response to oxidative stress, regulation of substrate adhesion-dependent cell spreading, heterotypic cell-cell adhesion, cellular response to acid chemicals, and regulation of smooth muscle cell proliferation, cell development, migration and proliferation, and transcription by RNA polymerase II (Figure 3). Enriched pathways, shown as dots in Figure 4 and listed by their adjusted p-value (p_{adj}), were analyzed across KEGG, Reactome and WikiPathways databases. Platelet aggregation (9) and activation (1), integrin signaling (8), PI3K-Akt (2, 12, 13), FoxO (3, 7) and mTOR (4, 13) signaling pathways and MAP kinase pathway activation (10) were the most statistically overrepresented. Using genes associated with the top GO terms, miRTarBase

analysis confirmed that they were targeted by miR-144-3p, miR-29c-3p, miR-1275, miR-590-3p, and miR-7-5p, which were among the 10 differentially expressed and validated miRNAs.

Discussion

Both the glandular and stromal compartments of eutopic endometrium from women with adenomyosis show alterations compared to healthy subjects (Vannuccini et al., 2017; Bulun et al., 2021; Zipponi et al., 2024a). However, the molecular mechanisms driving crosstalk between ESCs and epithelial glands, along with paracrine signaling underlying lesion development and progression, remain poorly understood. To our knowledge, this is the first study to comprehensively isolate and characterize stroma-derived exosomes from women with adenomyosis, thereby shedding light on their potential involvement in disease pathogenesis.

Successful isolation of exosomes was confirmed by size analysis and the presence of known transmembrane biomarkers CD9 and CD81. miRNA transcriptomic profiling of secreted exosomes from 14 samples revealed potential miRNA candidates showing different expression between adenomyosis and healthy subjects in the menstrual phase, suggesting a novel hypothesis on the potential role of menstruation in lesion establishment and progression. Among the miRNAs examined, miR-132-5p, miR-451a and miR-99a-5p were upregulated, while miR-431-3p, miR-29c-39, miR-337-5p, miR-144-3p, miR-590-3p, miR-1275 and miR-7-5p were downregulated in adenomyosis samples during the menstrual phase compared to controls. The identified miRNAs, which target genes crucial to cell proliferation, migration and survival, exhibit potential regulatory significance in the pathogenesis of the disease. This is further corroborated by an earlier study by Juárez-

Barber et al., where these same genes, including IGF1R, PLAG1, PTEN, MYC, YOD1 and ZNF264, were singled out as prominent targets of adenomyosis-related miRNAs (Juárez-Barber et al., 2023). In line with these findings, other possible players, like ZEB1, MMP-2 and BCL2 previously associated with cell dynamics in adenomyosis (Guo et al., 2022; Yu et al., 2021; Li et al., 2019a), were encountered in our study, thereby reinforcing the notion of a complex network of miRNA-mediated regulation in disease progression. Having confirmed the hypothesis that miRNA exosome cargo may play a role in crosstalk between stromal and epithelial compartments in the pathogenesis of adenomyosis, we were seeking to explore how menstruation might influence lesion establishment and progression.

Role of platelets

During menstruation, shedding of the endometrial lining involves significant vascular injury and bleeding, which naturally leads to platelet activation. This intensifies inflammation, promoting growth and survival of ectopic endometrial cells. The presence of activated platelets in both groups in this study is most likely a normal consequence of menstruation rather than an indicator of adenomyosis pathogenesis. Nevertheless, elevated markers of platelet activation were found in menstrual blood from women with adenomyosis, explaining why platelets may participate in the pathogenesis of the disease during menstruation by promoting cell growth and survival (Guo et al., 2023). However, reported findings on the role of platelets in the pathophysiological process of adenomyosis have been inconsistent (Liu et al., 2016; Guo et al., 2020; Mosele et al., 2021; Maybin and Critchley, 2009).

PI3K/Akt/mTOR pathway

Enriched pathways found in this study like PI3K/Akt and FoxO, which are critical to cell survival and angiogenesis as well as apoptosis and response to oxidative stress, further support the theory of growth of ectopic endometrial tissue into the myometrium (Stratopoulou et al., 2021). Estrogen stimulation of the PI3K/Akt/mTOR pathway, known to be aberrantly activated in adenomyosis (Driva et al., 2022; Xue et al., 2013; Guo et al., 2015), promotes endometrial epithelial cell invasion and migration, illustrating the complex interplay of hormonal and molecular mechanisms during menstruation in adenomyosis (Donnez et al., 2021a). The PI3K/Akt/mTOR pathway can also be activated by downstream integrin signaling cascades.

Integrins in endometrial cells

Enrichment of integrin signaling during menstruation suggests its potential involvement in endometrial repair and regeneration by mediating attachment of new cells to the underlying matrix, thereby aiding in cell interactions and cell-extracellular matrix adhesion in response to endometrial shedding. In adenomyosis, the same integrin-mediated processes may be hijacked, with abnormally expressed integrins in ectopic endometrial cells becoming more invasive, leading to formation of adenomyotic lesions (Xiao et al., 2013).

miR-451a

miR-451a has been suggested as a promising therapeutic target for endometriosis (Cosar et al., 2016; Li et al., 2019b), a disease that shares both pathogenic and clinical features with adenomyosis, and this study does indeed point to a potential shared regulatory mechanism. miR-451a is also associated with changes in progesterone values in the endometrium, indicating its possible involvement in modulating endometrial receptivity through progesterone-related pathways (Li et al., 2011). This is particularly important as

progesterone plays a crucial role in regulating the menstrual cycle and pregnancy, and dysregulation of its pathways is implicated in both diseases. miR-451a may contribute to progesterone resistance, where ectopic endometrial tissues exhibit a reduced response to progesterone's regulatory effects. This resistance disrupts normal endometrial function, contributing to impaired receptivity, abnormal menstrual cycles and disease progression (Donnez and Dolmans, 2021b). In adenomyosis, miR-451a levels were higher in ectopic lesions than in normal endometrium (Guo et al., 2015; Tang et al., 2023).

Summary

To sum up, the most overrepresented pathways targeted by miRNA exosome cargo secreted by ESCs from women with adenomyosis in the menstrual phase are mainly involved in endometrial cell survival, enhanced proliferation, angiogenesis, apoptosis and oxidative stress responses.

Strengths and limitations

The present study is highly informative and intended as a resource-type foundational work, having both strengths and limitations. The combination of NGS and validation through qPCR offers several strong points that complement each other, providing a comprehensive approach to studying miRNA expression. Specifically, NGS allows for unbiased, genome-wide profiling of miRNAs, bringing to light detectable miRNAs in samples and characterizing them in relation to adenomyosis. The main drawbacks of the study are sample size, diversity and representation due to limited availability of endometrial biopsies in the menstrual phase. We acknowledge that use of 2D in vitro culture systems may affect the phenotype of endometrial cells and fail to replicate the complex 3D structure and microenvironment of the native endometrium. This approach cannot capture key interactions between immune cells, blood vessels and the dynamic

hormonal changes that occur throughout the menstrual cycle, which are essential to understanding endometrial physiology and pathology.

Conclusion

By focusing for the first time on menstruation-specific molecular mechanisms, this preliminary study sheds light on the potential role of ESC paracrine signaling in adenomyosis lesion development and progression. Our findings suggest that intercellular communication during menstruation may play a pivotal role in driving epithelial glands into the myometrium. This concept aligns with theories in endometriosis research, where retrograde menstruation has been proposed as a mechanism for lesion development (Burney et al., 2012). An enhanced understanding of the role of menstruation in disease pathogenesis points to the critical influence of ESC signaling in the establishment of adenomyotic lesions. Furthermore, this foundational work reveals key data on intercellular communication mediated by stroma-derived exosomes and their miRNA cargo, suggesting possible novel regulatory pathways in the pathogenesis of the disease. More research is needed to elucidate the complex mechanisms involved in the crosstalk between ESCs and epithelial glands in the endometrium and how they drive adenomyotic lesion establishment. This information is crucial to developing more targeted and effective clinical treatments, addressing both the symptoms and underlying causes of the disorder. Having laid the ground with our data, future studies should seek to validate these findings in larger cohorts and apply functional assays to confirm the influence of ESCs and their involvement in disease development. This could significantly impact diagnostic and therapeutic approaches to this challenging condition.

Data availability statement

All data supporting this article are provided in the main body and are available in the online supplementary information. Raw data underlying miRNA sequencing are available in GSE281678 at https://www.ncbi.nlm.nih.gov/geo/query/acc.cgi?acc=GSE281678.

Acknowledgements

Library preparation and sequencing, as well as primary processing of sequenced data, were performed by Qiagen Genomic Services.

The authors thank Professor C. Pierreux (De Duve Institute) for providing the ultracentrifuge used in this study, and Mira Hryniuk, B.A., for reviewing the English language of the article.

Authors' roles

M.Z.: Conceptualization and design, sample collection and processing, methodology and experiment execution, formal analysis and interpretation of data, writing of original draft. L.C.: Formal analysis and interpretation of data, data curation, writing: review and editing. A.C.: Methodology. C.A.S.: Sample collection and methodology. H.S.T.: Interpretation of data, writing" review and editing. M-M.D.: Formal analysis and interpretation of data, supervision, writing" review and editing.

Funding

This study was supported by the Fonds National de la Recherche Scientifique de Belgique (FNRS) FC 52391 (to M.Z.), Scientific Collaborator Mandate (to L.C.), 5/4/150/5 (to M.M.D.), PDR-T.0171.21 (to A.C.), FC 39041 (to C.A.S.), private funding through the Fondation Saint-Luc (to M.M.D.), and the Hoover Seed Fund of UCLouvain (grant 2023) (to M.M.D.).

Conflict of interest

The authors have nothing to disclose.

References

Antero MF, Ayhan A, Segars J, Shih IM. Pathology and pathogenesis of adenomyosis. *Semin Reprod Med* 2020;**38**:108–118.

Bourdon M, Santulli P, Jeljeli M, Vannuccini S, Marcellin L, Doridot L, Petraglia F, Batteux F, Bulun SE, Yildiz S et al. Adenomyosis pathogenesis: insights from next-generation sequencing. *Hum Reprod Update* 2021;**27**(6):1086-1097.

Burney RO, Giudice LC. Pathogenesis and pathophysiology of endometriosis. *Fertil Steril* 2012;**98**(3):511–9.

Chapron C, Tosti C, Marcellin L, Bourdon M, Lafay-Pillet MC, Millischer AE, Streuli I, Borghese B, Petraglia F, Santulli P. Relationship between the magnetic resonance imaging appearance of adenomyosis and endometriosis phenotypes. *Hum Reprod* 2017;**32**(7):1393-1401.

Chapron C, Vannuccini S, Santulli P, Abrão MS, Carmona F, Fraser IS, Gordts S, Guo SW, Just PA, Noël JC et al. Diagnosing adenomyosis: an integrated clinical and imaging approach. *Hum Reprod Update* 2020;**26**(3):392-411.

Chen YJ, Li HY, Huang CH, Twu NF, Yen MS, Wang PH, Chou TY, Liu YN, Chao KC, Yang MH. Oestrogen-induced epithelial–mesenchymal transition of endometrial epithelial cells contributes to the development of adenomyosis. *J Path* 2010;**222**:261–270.

Chen D, Qiao H, Wang Y, Ling Zhou, Yin N, Fang L, Wang Z. Adenomyosis-derived extracellular vesicles endow endometrial epithelial cells with an invasive phenotype through epithelial-mesenchymal transition. *Genes Dis* 2020;**7**:636–648.

Cheng WX, Wei SB, Zhou Y, Shao Y, Li MY. Exosomes: potential diagnostic markers and drug carriers for adenomyosis. *Front Pharmacol* 2023;**14**:1216149.

Cosar E, Mamillapalli R, Ersoy GS, Cho S, Seifer B, Taylor HS. Serum microRNAs as diagnostic markers of endometriosis: a comprehensive array-based analysis. *Fertil Steril* 2016;**106**(2):402-9.

d'Argent M, Stratopoulou CA, Cussac S, Camboni A, Jadoul P, Donnez J, Dolmans MM. Are lower levels of apoptosis and autophagy behind adenomyotic lesion survival? *Reprod Biomed Online* 2023;**47**(3):103248.

Defrère S, Van Langendonckt A, Moulin P, Befahy P, Gonzalez D, Martinez-Madrid B, Dolmans MM, Donnez J. Human endometrial epithelial cells constitutively express more intercellular adhesion molecule (ICAM)-1 than endometrial stromal cells in culture. *Am J Reprod Immunol* 2005;**54**(1):5-12.

Donnez J, Stratopoulou CA, Dolmans MM. Uterine Adenomyosis: From Disease Pathogenesis to a New Medical Approach Using GnRH Antagonists. *Int J Environ Res Public Health* 2021a;**18**(19):9941.

Donnez J, Dolmans MM. Endometriosis and Medical Therapy: From Progestogens to Progesterone Resistance to GnRH Antagonists: A Review. *J Clin Med* 2021b;**10**(5):1085.

Driva TS, Schatz C, Sobočan M, Haybaeck J. The Role of mTOR and eIF Signaling in Benign Endometrial Diseases. *Int J Mol Sci* 2022;**23**(7):3416.

Esfandyari S, Elkafas H, Chugh RM, Park HS, Navarro A, Al-Hendy A. Exosomes as Biomarkers for Female Reproductive Diseases Diagnosis and Therapy. *Int J Mol Sci* 2021;**22**(4):2165.

García-Solares J, Donnez J, Donnez O, Dolmans MM. Pathogenesis of uterine adenomyosis: invagination or metaplasia? *Fertil Steril* 2018;**109**(3):371-379.

Guo Y, Lang X, Lu Z, Wang J, Li T, Liao Y, Jia C, Zhao W, Fang H. MiR-10b directly targets ZEB1 and PIK3CA to curb adenomyotic epithelial cell invasiveness via upregulation of E-Cadherin and inhibition of Akt phosphorylation. *Cellular Physiology and Biochemistry* 2015;**35**(6):2169–2180.

Guo, SW. The Pathogenesis of Adenomyosis vis-à-vis Endometriosis. *J Clin Med* 2020;**9**:485.

Guo Y, Wang J, Jia C, Liao Y. SKP2 regulates ZEB1 expression and stimulates eutopic endometrial stromal cell invasion and proliferation of adenomyosis. *Reprod Biol* 2022;**22**(1):100578.

Guo SW. The Role of Platelets in the Pathogenesis and Pathophysiology of Adenomyosis. *J Clin Med* 2023;**12**(3):842.

Juárez-Barber E, Segura-Benítez M, Carbajo-García MC, Bas-Rivas A, Faus A, Vidal C, Giles J, Labarta E, Pellicer A, Cervelló I et al. Extracellular vesicles secreted by adenomyosis endometrial organoids contain miRNAs involved in embryo implantation and pregnancy. *Reprod Biomed Online 2023*;**46**(3):470-481.

Khan KN, Kitajima M, Hiraki K, Fujishita A, Nakashima M, Masuzaki H. Involvement of Hepatocyte Growth Factor-Induced Epithelial-Mesenchymal Transition in Human Adenomyosis. *Biol Reprod* 2015;**92**(2):35.

Li R, Qiao J, Wang L, Li L, Zhen X, Liu P, Zheng X. MicroRNA array and microarray evaluation of endometrial receptivity in patients with high serum progesterone levels on the day of hCG administration. *Reprod Biol Endocrinol* 2011;**9**:29.

Li J, Yanyan M, Mu L, Chen X, Zheng W. The expression of Bcl-2 in adenomyosis and its effect on proliferation, migration, and apoptosis of endometrial stromal cells. *Pathol Res Pract* 2019a;**215**(8):152477.

Li M, Zhou Y, Taylor HS. MiR-451a inhibition reduces established endometriosis lesions in mice. *Reprod Sci* 2019b;**26**(11):1506-1511.

Liu X, Shen M, Qi Q, Zhang H, Liu SW. Corroborating evidence for platelet-induced epithelial-mesenchymal transition and fibroblast-to-myofibroblast transdifferentiation in the development of adenomyosis. *Hum Reprod* 2016;**31**:734–749.

Maybin J, & Critchley H. Repair and regeneration of the human endometrium. *Expert Rev Obstet Gynecol* 2009;**4**(3):283–298.

Mosele S, Stratopoulou CA, Camboni A, Donnez J, Dolmans MM. Investigation of the role of platelets in the aetiopathogenesis of adenomyosis. *Reprod Biomed Online* 2021;**42**:826–834.

Naftalin J, Hoo W, Pateman K, Mavrelos D, Holland T, Jurkovic D. How common is adenomyosis? A prospective study of prevalence using transvaginal ultrasound in a gynaecology clinic. *Hum Reprod* 2012;**27**(12):3432-9.

Nguyen HP, Simpson RJ, Salamonsen LA, Greening DW. Extracellular Vesicles in the intrauterine environment: challenges and potential functions. *Biol Reprod* 2016;**95**(5):109.

Pinzauti S, Lazzeri L, Tosti C, Centini G, Orlandini C, Luisi S, Zupi E, Exacoustos C, Petraglia F. Transvaginal sonographic features of diffuse adenomyosis in 18-30-year-old nulligravid women without endometriosis: association with symptoms. *Ultrasound Obstet Gynecol* 2015;**46**(6):730-6.

Stratopoulou CA, Donnez J, Dolmans MM. Origin and Pathogenic Mechanisms of Uterine Adenomyosis: What Is Known So Far. *Reprod Sci* 2021;**28**(8):2087-2097.

Stratopoulou CA, Cussac S, d'Argent M, Donnez J, Dolmans MM. M2 macrophages enhance endometrial cell invasiveness by promoting collective cell migration in uterine adenomyosis. *Reprod Biomed Online* 2023;**46**(4):729-738.

Tang Y, Ponandai-Srinivasan S, Frisendahl C, Andersson JK, Pavone D, Stewart EA, Lalitkumar PGL, Korsching E, Bogavarappu NR, Gemzell-Danielsson K. Bromocriptine inhibits proliferation in the endometrium from women with adenomyosis. *Front Endocrinol* 2023;**14**:1026168.

Upson K and Missmer SA. Epidemiology of Adenomyosis. *Semin Reprod Med* 2020;**38**(2-03):89-107.

Vannuccini S, Tosti C, Carmona F, Huang SJ, Chapron C, Guo SW, Petraglia F. Pathogenesis of adenomyosis: an update on molecular mechanisms. *Reprod BioMed Online* 2017;**35**(5):592–601.

Vannuccini S and Petraglia F. Recent advances in understanding and managing adenomyosis. *F1000Res* 2019;**8**:F1000 Faculty Rev-283.

Welsh JA, Goberdhan DCI, O'Driscoll L, Buzas EI, Blenkiron C, Bussolati B, Cai H, Di Vizio D, Driedonks TAP, Erdbrügger U et al. Minimal information for studies of extracellular vesicles (MISEV2023): From basic to advanced approaches. *J Extracell Vesicles* 2024;**13**(2):e12404.

Xiao Y, Li T, Xia E, Yang X, Sun X, Zhou Y. Expression of integrin β3 and osteopontin in the eutopic endometrium of adenomyosis during the implantation window. *Eur J Obstet Gynecol Reprod Biol* 2013;**170**(2):419-22.

Xue J, Zhang H, Liu W, Liu M, Shi M, Wen Z, Li C. Metformin inhibits growth of eutopic stromal cells from adenomyotic endometrium via AMPK activation and subsequent inhibition of AKT phosphorylation: a possible role in the treatment of adenomyosis. *Reprod* 2013;**146**(4):397-406.

Yang JH, Wu MY, Chen CD, Chen MJ, Yang YS, Ho HN. Altered apoptosis and proliferation in endometrial stromal cells of women with adenomyosis. *Hum Reprod* 2007;**22**(4):945-52.

Yu K, Cui S, Xue T. LncRNA MIR22HG is downregulated in adenomyosis and upregulates miR-2861 through demethylation to inhibit endometrial cell proliferation. *J Obstet Gynaecol Res* 2021;**47**(5):1837-1845.

Zhai J, Vannuccini S, Petraglia F, Giudice LC. Adenomyosis: Mechanisms and Pathogenesis. *Semin Reprod Med* 2020;**38**(2-03):129-143.

Zhai J, Li S, Sen S, Vallvé-Juanico J, Irwin JC, Vo KC, Wan J, Du Y, Chen ZJ, Giudice LC. Transcriptomic analysis supports collective endometrial cell migration in the pathogenesis of adenomyosis. *Reprod Biomed Online* 2022;**45**(3):519-530.

Zhang, Y., Liu, Y., Liu, H. Exosomes: biogenesis, biologic function and clinical potential. *Cell Biosci* 2019;**9**:19.

Zhou C, Zhang T, Liu F, Zhou J, Ni X, Hou R, Shi Z. The differential expression of mRNAs and long noncoding RNAs between ectopic and eutopic endometria provides new insights into adenomyosis. *Mo BioSyst* 2015;**12**:362–370.

Zipponi M, Cacciottola L, Dolmans MM. Overview of crosstalk between stromal and epithelial cells in the pathogenesis of adenomyosis and shared features with deep endometriotic nodules. *Human Reprod* 2024a;**39**(8):1608-1617.

Zipponi M, Lee DY, Stratopoulou CA, Camboni A, Cacciottola L, Dolmans MM. Characterization of microRNA exosome content from endometrioma wall in vitro culture. *Fertil Steril* 2024b;**122**(1):174-177.

659 **Figure legends**

660 **Graphical abstract. Stroma-derived exosome characterization in women with**
661 **adenomyosis.**

662 **Figure 1. Exosome characterization**

663 A) Particle size and concentration assessed by nanoparticle tracking analysis (NTA).
664 B) Morphological appearance of exosomes isolated by ultracentrifugation. Transmission
665 electron microscopy (TEM) image. Original magnification: 20,000. Scale bar: 0.2 μm.
666 C) Exosome biomarker evaluation (CD9 and CD81) by flow cytometry.

667 **Figure 2. Dysregulated miRNAs**

668 There were 38 miRNAs selected based on sequencing data as shown by all coloured dots
669 (small and large) in the volcano plot. Red dots represent the 14 miRNAs that are more
670 widely expressed in adenomyosis samples in the menstrual phase compared with
671 controls. Blue dots symbolize the 22 miRNAs that are less widely expressed. Grey dots
672 show no changes in miRNA expression. The ten miRNAs found to be significantly
673 differently expressed by qPCR are indicated by larger dots (3 red and 7 blue). The Y-axis
674 represents p-values ($-\log_{10}$) and the X-axis represents the fold change ($\log_2$).

675 **Figure 3. GO enrichment analysis**

676 Gene Ontology (GO) enrichment analysis carried out with ShinyGO v0.80. GO terms for
677 the biological process category of predicted target genes are listed based on their fold
678 enrichment, the percentage of differentially expressed genes belonging to a pathway,
679 divided by the corresponding percentage of genes in the background. Greater numbers
680 of genes involved in a specific pathway suggest lower specificity (yellow), while fewer
681 genes indicate higher target specificity (violet).

682 **Figure 4. Functional enrichment analysis**

683 Enrichment overrepresentation analysis results of predicted target genes in the first 10
684 Gene Ontology (GO) terms tested against KEGG, Reactome (REAC) and WikiPathways
685 (WP). The most significant pathways are highlighted (false discovery rate (FDR) <0.01)
686 and ordered by the adjusted p-value (p_{adj}) of differentially expressed genes. The Y-axis
687 represents Benjamini-Hochberg-corrected p-values ($-\log_{10}$) and the X-axis represents the
688 functional terms that were grouped and colour-coded by data source.

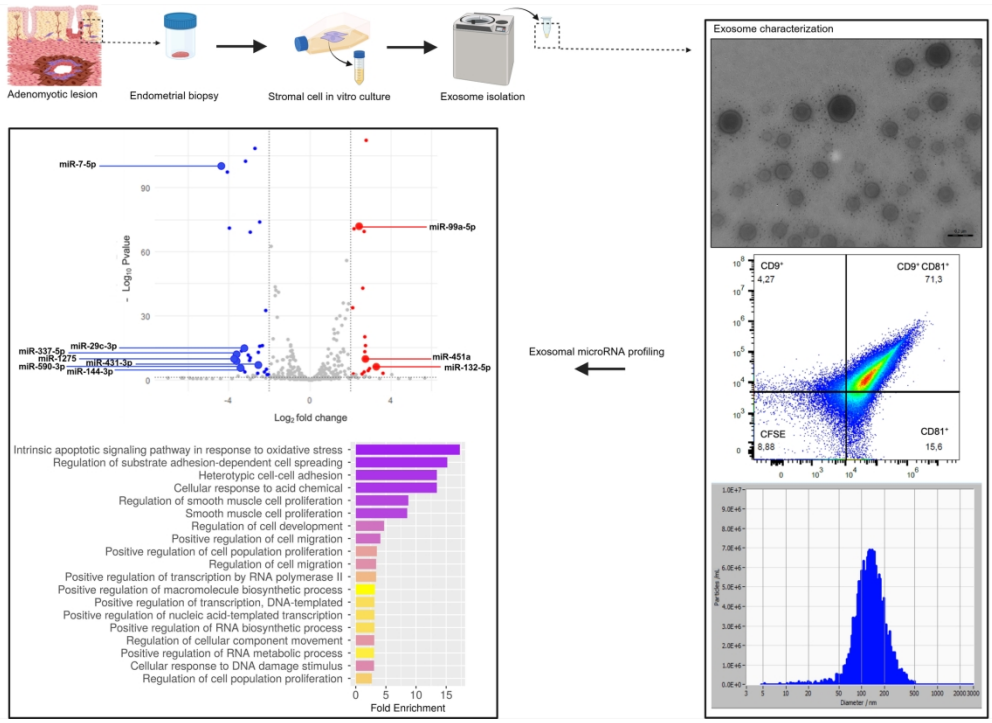

179x128mm (300 x 300 DPI)

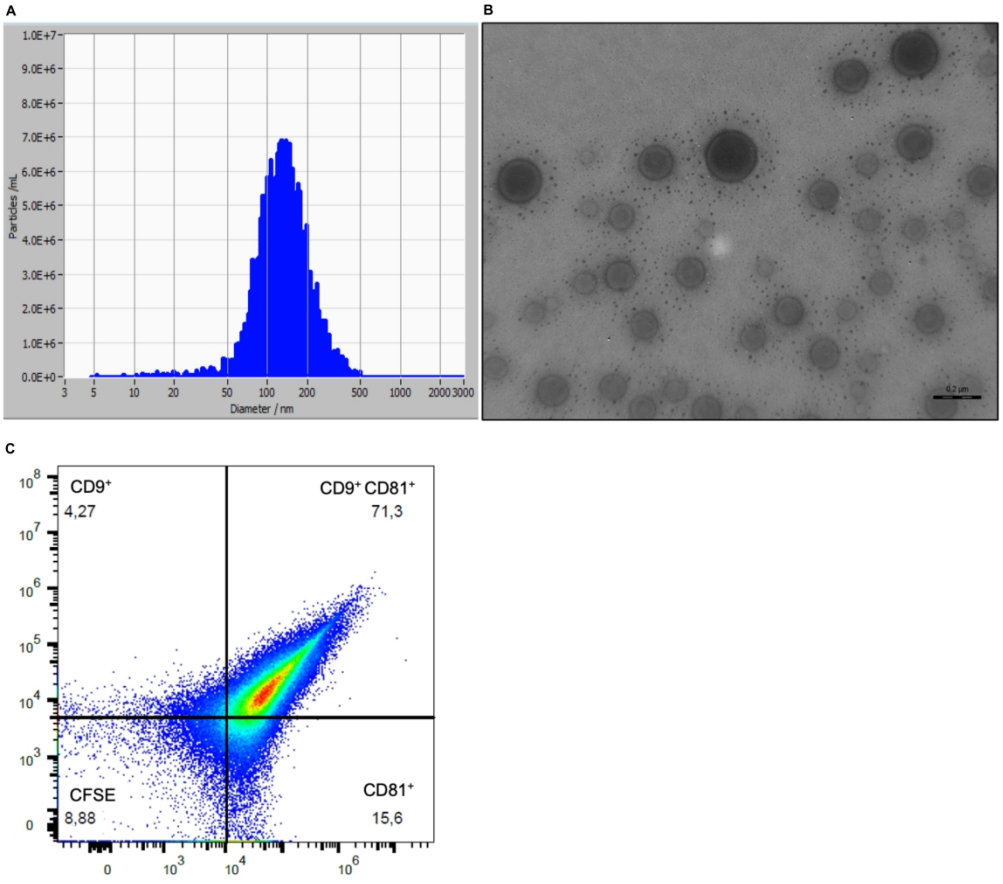

Figure 1. Exosome characterization
A) Particle size and concentration assessed by NTA.
B) Morphological appearance of exosomes isolated by ultracentrifugation. TEM image. Original magnification: 20,000. Scale bar: 0.2 μm.
C) Exosome biomarker evaluation (CD9 and CD81) by flow cytometry.

200x200mm (600 x 600 DPI)

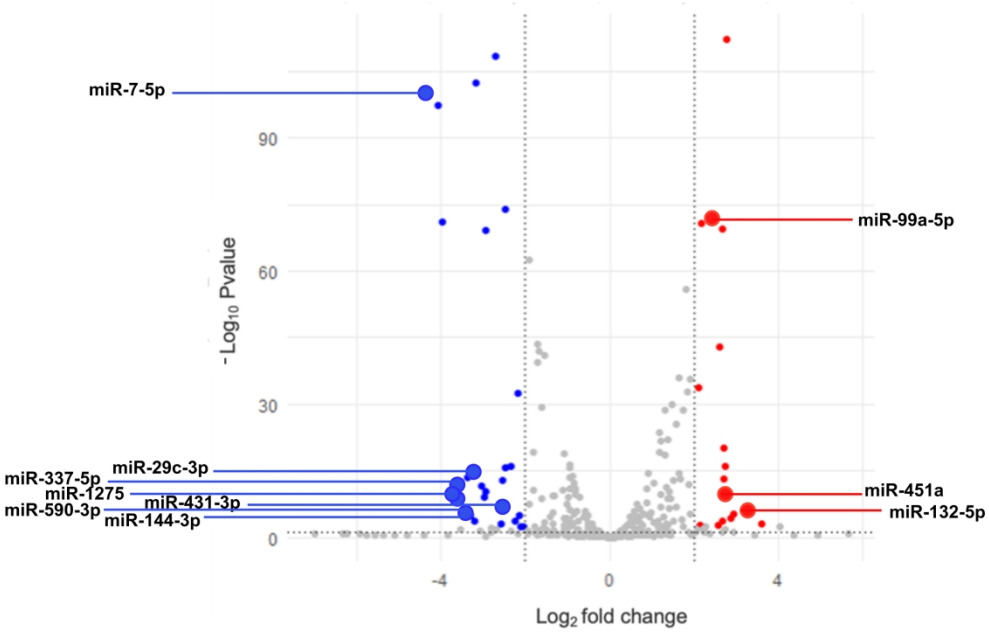

Figure 2. Dysregulated miRNAs
Thirty-eight miRNAs selected based on sequencing data are shown as dots in the volcano plot. Red dots represent the 14 miRNAs that are more widely expressed in adenomyosis samples in the menstrual phase compared with controls. Blue dots symbolize the 22 miRNAs that are less widely expressed. Grey dots show no changes in miRNA expression. MiRNAs found to be significantly differently expressed by qPCR are indicated by larger dots. The Y-axis represents p-values (-log10) and the X-axis represents the fold change (log2).

254x177mm (300 x 300 DPI)

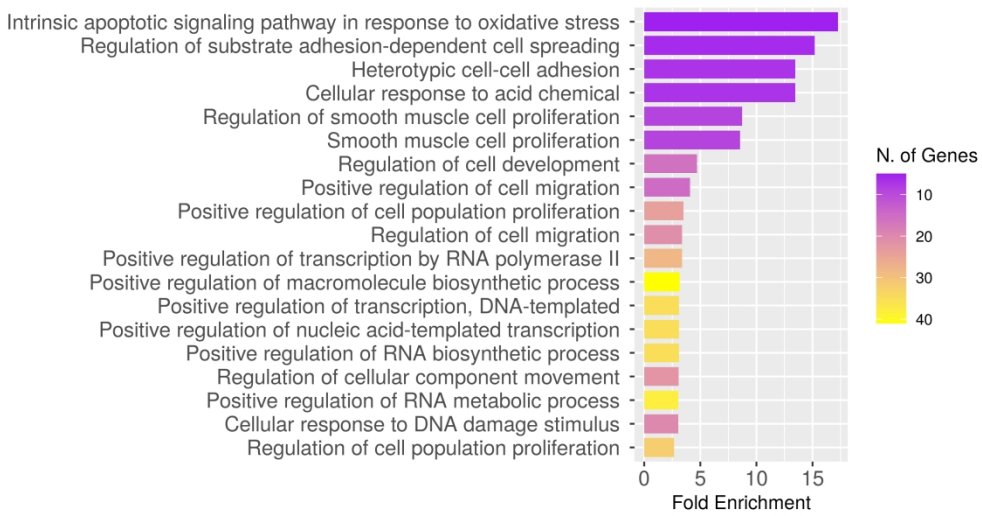

Figure 3. GO enrichment analysis
GO enrichment analysis carried out with ShinyGO v0.80. GO terms for the biological process category of predicted target genes are listed based on their fold enrichment, the percentage of differentially expressed genes belonging to a pathway, divided by the corresponding percentage of genes in the background. Greater numbers of genes involved in a specific pathway suggest lower specificity (yellow), while fewer genes indicate higher target specificity (violet).

121x64mm (600 x 600 DPI)

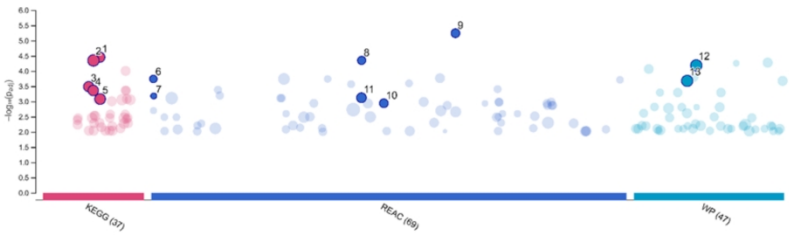

Term name	Adjusted p-value	ID	Database
Platelet aggreation (plug formation)	$5.69x10^{-5}$	9	REAC
Platelet activation	$3.51x10^{-5}$	1	KEGG
Integrin singaling	$4.45x10^{-5}$	8	REAC
PI3K-Akt signaling pathway	$4.46x10^{-5}$	2	KEGG
PI3K-Akt signaling pathway	$6.52x10^{-5}$	12	WP
AKT phosphorylates targets in the cytosol	$1.81x10^{-4}$	6	REAC
Focal adhesion PI3K-Akt-mTOR signaling pathway	$2.1x10^{-4}$	13	WP
FoxO signaling pathway	$3.2x10^{-4}$	3	KEGG
mTOR signaling pathway	$4.34x10^{-4}$	4	KEGG
AKT-mediated inactivation of FOXO1A	$6.58x10^{-4}$	7	REAC
Integrin cell surface interactions	$7.5x10^{-4}$	11	REAC
Neutrophil extracellular trap formation	$8.26x10^{-4}$	5	KEGG
MAP2K and MAPK activation	$1.14x10^{-3}$	10	REAC

Figure 4. Functional enrichment analysis
Enrichment overrepresentation analysis results of predicted target genes in the first 10 GO terms tested against KEGG, Reactome (REAC) and WikiPathways (WP). The most significant pathways are highlighted (FDR <0.01) and ordered by the adjusted p-value (padj) of differentially expressed genes. The Y-axis represents Benjamini-Hochberg-corrected p-values (-log10) and the X-axis represents the functional terms that were grouped and color-coded by data source.

299x209mm (300 x 300 DPI)

1 **Table 1. Validation of miRNA expression**

	Mature ID	P value	Fold change
Log_2 fold change >2	**hsa-miR-132-5p**	**0.026**	**8.57**
	hsa-miR-99a-5p	**0.029**	**2.16**
	hsa-miR-451a	**0.039**	**3.17**
	hsa-miR-1468-5p	0.051	7.63
	hsa-miR-3605-5p	0.052	13.53
	hsa-miR-130b-5p	0.054	3.22
	hsa-miR-196a-5p	0.055	4.19
	hsa-miR-10b-5p	0.055	2.21
	hsa-miR-150-5p	0.065	3.32
	hsa-miR-4636	0.131	3.60
	hsa-miR-940	0.135	1.82
	hsa-miR-100-5p	0.176	2.26
	hsa-miR-204-3p	0.177	2.90
	hsa-miR-214-3p	0.182	1.62
	hsa-miR-3182	0.378	2.05
	hsa-miR-629-5p	0.526	1.16
	hsa-miR-139-5p	0.959	1.35
Log_2 fold change <-2	**hsa-miR-337-5p**	**0.029**	**-6.02**
	hsa-miR-590-3p	**0.035**	**-5.77**
	hsa-miR-29c-3p	**0.008**	**-5.61**
	hsa-miR-144-3p	**0.029**	**-3.36**
	hsa-miR-7-5p	**0.011**	**-2.91**
	hsa-miR-431-3p	**0.038**	**-2.35**
	hsa-miR-1275	**0.029**	**-1.71**
	hsa-miR-136-3p	0.073	-2.10
	hsa-miR-1-3p	0.14	-1.76
	hsa-miR-376a-3p	0.066	-2.27
	hsa-miR-497-5p	0.317	-2.02
	hsa-miR-4443	0.392	-1.33
	hsa-miR-130a-3p	0.080	-7.32
	hsa-miR-15a-5p	0.067	-3.24

	hsa-miR-340-5p	0.164	-1.89
	hsa-miR-29a-3p	0.072	-3.47
	hsa-miR-27a-3p	0.063	-5.13
	hsa-miR-376b-3p	0.031	-3.08
	hsa-miR-424-5p	0.208	-4.89
	hsa-miR-1185-1-3p	0.38	-2.54
	hsa-miR-29b-3p	0.186	-2.43

miRNA differential expression validation in adenomyosis and healthy subjects in the menstrual phase by qPCR. Significantly differently expressed miRNAs (n=10) are highlighted in bold. Specifically miR-132-5p, miR-451a and miR-99a-5p are upregulated in adenomyosis, while miR-431-3p, miR-29c-39, miR-337-5p, miR-144-3p, miR-590-3p, miR-1275 and miR-7-5p are downregulated.